Journal of Asian Ceramic Societies

ISSN: (Print) (Online) Journal homepage: www.tandfonline.com/journals/tace20

Effects of surfactants/stabilizing agents on the microstructure and properties of porous geopolymers by direct foaming

Yingjie Qiao, Xinyu Li, Chengying Bai, Hongqiang Li, Jinghao Yan, Yi Wang, Xiaodong Wang, Xiaohong Zhang, Ting Zheng & Paolo Colombo

To cite this article: Yingjie Qiao, Xinyu Li, Chengying Bai, Hongqiang Li, Jinghao Yan, Yi Wang, Xiaodong Wang, Xiaohong Zhang, Ting Zheng & Paolo Colombo (2021) Effects of surfactants/stabilizing agents on the microstructure and properties of porous geopolymers by direct foaming, Journal of Asian Ceramic Societies, 9:1, 412-423, DOI: 10.1080/21870764.2021.1873482

To link to this article: https://doi.org/10.1080/21870764.2021.1873482

Published online: 15 Jan 2021.

JOURNAL OF ASIAN CERAMIC SOCIETIES
2021, VOL. 9, NO. 1, 412–423
https://doi.org/10.1080/21870764.2021.1873482

Effects of surfactants/stabilizing agents on the microstructure and properties of porous geopolymers by direct foaming

Yingjie Qiao[a], Xinyu Li[a], Chengying Bai[a], Hongqiang Li[b], Jinghao Yan[a], Yi Wang[a], Xiaodong Wang[a], Xiaohong Zhang[a], Ting Zheng[a] and Paolo Colombo[c,d]

[a]Key Laboratory of Superlight Materials and Surface Technology, Ministry of Education, College of Materials Science and Chemical Engineering, Harbin Engineering University, Harbin, China; [b]College of Civil Engineering, Hunan University, Changsha, China; [c]Department of Industrial Engineering, University of Padova, Padova, Italy; [d]Department of Materials Science and Engineering, The Pennsylvania State University, University Park, PA, USA

ABSTRACT

Metakaolin-based porous geopolymers were synthesized by direct foaming using various surfactants/stabilizing agents with or without chemical pore-forming agent (hydrogen peroxide). The effects of surfactants/stabilizing agents and solid loading on their pore morphology, density, porosity, and some properties, such as thermal conductivity and compression strength, were investigated. Experimental data and different theoretical models were successfully applied to evaluate both compression strength (σ) and effective thermal conductivity (λ) as a function of porosity (ε). Porous geopolymers with higher ε presented both a lower value of mechanical strength and improved thermal conductivity performance. The variation of σ with ε could be well described by the minimum solid area (MSA) model, and the variation of λ with ε was found to be more accurately described using a universal model derived from the five basic models.

ARTICLE HISTORY
Received 12 August 2020
Accepted 4 January 2021

KEYWORDS
Porous geopolymers; metakaolin; peroxide; surfactants; thermal conductivity

1. Introduction

Porous geopolymers (PGs) is one of the fastest-growing research area in the field of porous inorganic non-metallic materials, because of the good global availability and low cost of the starting materials, the possibility of producing components without requiring a sintering step, and their promising properties (high mechanical strength, low thermal conductivity, very good chemical stability etc.) [1–3]. The manufacturing of such components has been motivated by a large number of potential applications, such as inorganic membrane and membrane supports [4–6], low-cost adsorbents [7–9], acoustic and thermal insulation [9,10], etc. A wide range of processing techniques (direct foaming method, replica route, sacrificial filler method, 3D printing, combined route, etc.) have been demonstrated for the fabrication of PGs over the last decade [1], with direct foaming method being the simplest and most promising for large-scale manufacturing. Aluminum powder (Al), silicon powder (Si) and other Si-containing materials (FeSi, SiC, silica fume), and hydrogen peroxide (H_2O_2) solution have been employed as chemical pore-foaming agents (CPFAs) for the fabrication of PGs [1]. H_2O_2 solution is more suitable compared with the use of metallic Si and Al due to the well-controllable decomposition of hydrogen peroxide and the possibility of homogeneously distributing the foaming agent within the geopolymer slurry [1,11,12]. Additionally, previous investigations have indicated that adding suitable surfactants or stabilizing agents (SAs) into the slurry benefits the stability of the wet foam and assists in controlling the amount of interconnected (open) porosity generated, i e., PGs with low density, high strength as well as controllable porosity can be achieved by the synergistic effect of CPFAs and SAs [1,[11].

Metakaolin (MK), derived from kaolin minerals after thermally treated, showed more consistent chemical compositions than fly ash and slag, and was widely used for geopolymer manufacture [1,[13].

Various of surfactants or stabilizing agents (SAs, when they combined with blowing agents) including protein [5], vegetable oils [11], Tween-80 [9], Triton X-100 [14], sodium dodecyl sulfate(SDS) [15], oleic acid [16], Sikas Lightcrete02 [17], sodium dodecyl benzene sulfonate (SDBS) [18–20], and other commercial surfactants (no chemical composition given) [21,22] etc., combined with or without H_2O_2 solution have been investigated to develop porous geopolymer components [1]. However, there are no comparative studies, to the best of our knowledge, aiming at assessing the effect of using different surfactants for the pore structure, mechanical and thermal properties of porous geopolymers while maintaining constant the composition of the geopolymer slurry.

CONTACT Chengying Bai chengyingbai@163.com Jichu Building 122, Nantong street No 145, College of Materials Science and Chemical Engineering, Harbin Engineering University, Harbin, Heilongjiang Province 150001, China
The online version of this article contains supplementary materials (**Table S1; Figs. S1-7**), which are available to authorized users.

In this study, porous metakaolin-based geopolymers (PMGs) were fabricated using different surfactants/SAs. Effects of different surfactants on total porosity, bulk density, cell size and cell size distribution, pore microstructure as well as mechanical and thermal properties of PMG samples were reported. Furthermore, the solid content in the slurry and the synergistic effect with chemical pore-forming agent with the different surfactants or stabilizing agents (SAs) were also investigated. The change in the thermal conductivity and compressive strength of PG materials as a function of the percentage of porosity was also investigated.

2. Experimental section

2.1. Raw materials

Metakaolin (MK, Chenyi, Henan, China), average particle size about 10 μm, was used as the raw aluminosilicate mineral material. The chemical composition of the MK provided by the supplier is given in Table 1.

LOI* = Loss of ignition

A 9.4 M NaOH solution (obtained by dissolving particulate sodium hydroxide from Fulu, Tianjin, China) and a sodium silicate solution (water glass, Dongyue federation, Shandong, China) with SiO_2:Na_2O mole ratio of 3.3 were well mixed to form the alkali activator solution. 3%w/w H_2O_2 solution, freshly diluted from 30%w/w aqueous H_2O_2 solution (Dongli chemical enterprise, Jiangsu, China) at room temperature, was used as CPFA. Previous studies [11] [14] showed that diluted hydrogen peroxide assisted in achieving a homogeneous pore structure. The information (trade name, classification, molecule composition, effective content, phase of the matter at ambient temperature, and supplier) of the six surfactants or stabilizing agents (SAs) used in this work are listed in Table 2.

2.2. Manufacturing process

Prior to the experiments, a starting suspension (SS) of geopolymer, with a theoretical oxide molar ratios: SiO_2/Al_2O_3 = 3.18, Na_2O/Al_2O_3 = 0.83, Na_2O/SiO_2 = 0.26, and H_2O/Na_2O = 16.45, was designed based on previous works [9,[11]. SS was obtained by mechanical mixing (paddle type mixer, OS-20, Dragonlab, Beijing, China) of the MK and the alkali activator solution for 40 min at 600 rpm. Here, the weight ratio of SAs in the SS was defined as x%, the weight fraction of additional H_2O_2 and H_2O in the SS was defined as y% and z%, respectively. The SAs (x = 3.15 wt%) were added into the SS stirring at 1200 rpm for 5 min. Then, H_2O_2 solution (y = 11 wt %) or additional water (z = 11 wt%) was added into the SS stirring another 5 min at 800 rpm. PGs only with H_2O_2 addition (PMGH) were also produced for blank samples.

After being prepared, the wet foams were cast into resin molds, the molds were sealed with polyethylene films to prevent the formation of drying cracks and put into an electric thermostat blast dryer (DHG-9076A, Jinghong, Shanghai, China). The curing temperature was initially fixed at 35°C (~24 h) to avoid rapid decomposition (H_2O_2) to ensure well-controlled pore formation, and then the samples were cured at 75°C for another 24 h to promote consolidation and further hardening through the completion of the geopolymerization reaction [9,11]. The dimensions of the resulting porous metakaolin-based geopolymer (PMG) samples were about ~15 ×~65× ~65 mm^3 after polishing.

2.3. Characterization

Thermal conductivity (λ) of the polished and dried PMG samples was characterized at ambient environment using the transient plane source method, using a hot-wire thermal properties analyzer (DRE-III, Xiangtan, China) [9,11]. Three cubic specimens were measured per each test, to ensure reproducibility and accuracy, and the average results are reported.

The original-polished specimens were cut into regular parallelepipeds (~15 ×~20× ~20 mm^3) and dried for further characterization. Uniaxial compressive strength (σ) was determined by using a WDW-100 universal material testing machine (Kexin, Changchun, China) at a rate of 1 mm/min, and the average compressive strength (standard deviation) of the specimens derived from five cubic specimens per mixture were reported. Stress–strain curves and elasticity modulus (E) were obtained after data analysis.

Table 1. Chemical composition (wt%) of the metakaolin.

SiO_2	Al_2O_3	Na_2O	K_2O	MgO	CaO	Fe_2O_3	TiO_2	LOI*
55.06	44.12	0.06	0.55	0.06	0.17	0.76	0.24	0.62

Table 2. Details of the six surfactants or stabilizing agents (SAs) used in this work.

Sample label	Trade name	Type	Molecule	Content (wt%)	Phase	Supplier
K12	K12	Anionic	Sodium dodecyl sulfate (SDS)	93	Solid	Lusen, Shandong,China
JFC	JFC-3	Nonionic	Isomeric octanol ethoxylates	99	Liquid	Lusen, Shandong,China
AK	AK-301	Amphoteric	Sodium cocoly glycinate	30	Liquid	Ankang, Liaoning,China
BC	BC	Cationic	Benzethonium chloride	99	Solid	Sunpu Biochem, Beijing,China
SP	Soup	-	-	-	Liquid	Miniso, Japan
PO	Palm oil	-	-	-	Liquid/Solid	Yihaijiali, Shanghai,China

The percentage values of total porosity or void fraction (ε) were analytically calculated based on the following formula (1) [23,24]:

$$\varepsilon = 100\%(1 - \rho_b/\rho_t) \quad (1)$$

where ρ_b is the bulk density of PMG determined by the simple geometric method (ratio between weight and geometrical volume) in accordance to ASTM C20-00. The ρ_t was the true density obtained using a water pycnometer in accordance to ASTM C604, and the mean ρ_t values of geopolymer samples were averaged over three measurements.

The fracture surface of PMG materials was assessed using desktop scanning electron microscope (SEM; Phenom pure+, Netherlands) with fixed light optical magnification range 20x and with high electron optical magnification range up to ~60,000x.

X-ray diffraction analysis was carried out on geopolymer powder using Cu kα radiation (1.54 Å) at 40 kV,150 mA, operated with 0.02° 2θ steps and a scan rate of 10 s per step (XRD, D/MAX-TTRIII, Rigaku Corporation, Japan). To identify the crystal structures, the obtained powder diffraction patterns were compared to the International Center for Diffraction Data (ICDD PDF2) database using the Match! software.

Fourier-transform infrared spectroscopy (FTIR) data were collected using an infrared spectrophotometer (Nicolet 6700, Thermo Scientific, Madison, USA). The IR spectra were gathered between 450 and 4000 cm^{-1} at room temperature with a KBr pellet.

The average cell size (d) and cell size distribution of PMGs were obtained via image analysis software (Nano Measurer 1.2) [11,25,26]. Data acquired from optic or SEM plane photographs analysis were firstly converted to three-dimensional values using the simple stereological equation [11,27]:

$$D_{sphere} = D_{circle}/0.785 \quad (2)$$

3. Results and discussion

3.1. X-Ray diffraction and infrared spectroscopy analysis

Figure 1(a) shows the XRD analysis results of the geopolymer (PMGH) and metakaolin. MK possessed a high content of amorphous phase (diffuse features located at 19–25 degree), and some anatase (TiO_2, PDF 00–073-1764) and quartz (SiO_2, PDF 01–087-2096) crystalline impurities. In the geopolymer, a new broad amorphous band in the 20–40 degree was detected, and the amorphous band centered at 28°was regarded as the typical diffuse hump for geopolymer (amorphous aluminosilicates) [13,16]. In comparison with MK, an obvious shift of the center of the humps from about ~22° to ~28° was observed. The presence of the new amorphous phase together with the shift of the center of the hump from about 22° to 28°, provides corroboratory evidence for the occurrence of the geopolymerization reaction during the synthesis of the material [28].

Figure 1(b) reports the FTIR data for the geopolymer and the pure MK. The characteristic bands of MK can be clearly observed at 1080, 802, 566, and 460 cm^{-1} [14,29–32]. The strong broad band with wavenumber centered at 1080 cm^{-1} is related to the stretching vibration of Si–O–Al and Si–O–Si [14,30], and previous works reported that this broad band from 1200 to 1000 cm^{-1} is caused by the overlapping of bands derived from dehydroxilated pyrophyllite [29,31]. Furthermore, the band at 802 cm^{-1} corresponds to the O–Al–O bending vibrations of AlO_4 tetrahedra [29,31], and the band with low intensity detected in the spectrum at 566 cm^{-1} belongs to the Si–O–Al bond in octahedral coordination [14,30].

For the geopolymer, the broad band from 3658 to 3180 cm^{-1} detected in the spectra can be assigned to stretching vibration of structural water and free water, and the small bands at 1651 and 714 cm^{-1} is attributed to the bending vibration of free water [14,31,33]. The occurrence of new correlative characteristic bands, the disappearance of the

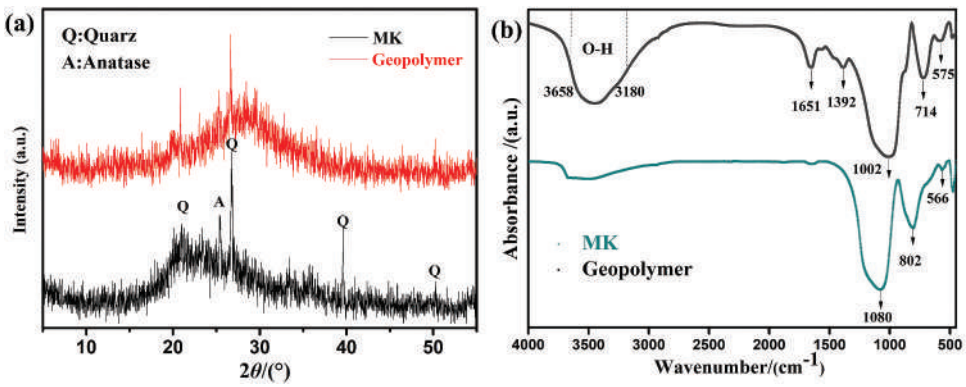

Figure 1. XRD patterns (a) and FTIR spectra (b) of metakaolin and geopolymer powders (PMGH).

band at 802 cm^{-1}, and the obvious shift of the center of broad bands from about 1080 toward 1002 cm^{-1}, compared with pure MK, jointly indicated the proceeding of the geopolymerization reaction and setting [14,30–32]. The new weak intensity of band located at 1392 cm^{-1} is assigned to the vibration of the C-O bond of carbonate groups by the atmospheric carbonation of the alkaline cations [32].

3.2. Pore microstructure

Porous geopolymers (PGs) were obtained by the direct foaming route using six different surfactants (SAs, 3.15 wt%; x = 3.15), with or without H_2O_2 as chemical pore foaming agent (CPFA). The introduction of a large amount of H_2O_2 (11 wt%; y = 11) to the starting suspension (SS) may have a significant effect on the fluidity. Therefore, samples with same amount of additional H_2O (11 wt%, z = 11) using different types of surfactants were also investigated. Figures 2–4 report the optical images (a–c) and (A-C), and SEM images (d–i) and (D-I) of the cellular solids produced using different types of SAs (amount of stabilizing agent set at x = 3.15) with and without fixed H_2O_2 content (y = 11) and fixed H_2O content (z = 11). To avoid repetition and retain clarity, **Table S1** lists the values of average cell size(d), relative density (ρ_b), compression strength (σ), total porosity (ε), elasticity modulus (E), and thermal conductivity(λ) for samples produced with different amounts of surfactant (x%), H_2O_2 (y%), and H_2O (z%).

Previous works [34–36] showed that the nature of the surfactant plays an important role in the fabrication of porous geopolymers by direct foaming. Indeed, different surfactants showed different foaming ability for the geopolymer slurry (see Figures 2–4 (a, a) (z = o) and Figures 2–4 (c, c) (z = 11)). The total porosity (ε/vol %) of porous samples varied with different surfactants, as follows: AKs (68) > K12s (60) > BCs (56) > POs (54) >JFCs (52) > SPs (50). Figures 2–4 (a, a) showed that the average cell size was also different between the six different porous samples. Based on the microscopy observations, the average cell size (d) and cell size distribution of PGs were computed using image analysis software. The cell size distribution was only partially reported (see Figure 5(d-i) for samples using both SAs and H_2O_2 (x = 3.15; y = 11; z = 0)) for the sake of brevity. The average cell size (d, in μm) of PGs with different types of surfactant seemingly followed a different order comparing with total porosity: POs (158) > SPs (142) > K12s (133)> JFCs (130) > AKs (118) > BCs (114), although the differences are virtually nonexistent when taking into account the standard deviation. Furthermore, the influence of the solid content in the slurry was also investigated. As it can be seen in Figure 2–4 (c,c), the decrease of solid content in the slurry (z = 11) results in the obvious increase of the total porosity for all types of surfactant, this increase with the decrease of solid content and the variation with different surfactant can be attributed to foam ability and foam stability [35,[37,38]. Generally, a solution (slurry) with lower surface tension of air-liquid interface and lower viscosity is beneficial to generate more foams, while higher viscosity and elasticity are help for foam stability [38].

It is interesting to observe that similar order (AKw (77) > K12w (75) > BCw(64) > JFCw (62) >POw (60)> SPw (54)) with the type of surfactant as that for the total porosity (ε/vol%). While the order of average cell size (d/μm) was changed as follows: K12w (316) > BCw (227) > AKw (223) > JFCw (220) > SPw (133) > POw (102), indicating a strong effect of the solid content on the obtained cell size. The obvious variation for porosity and pore structure for the porous samples with different surfactant could be simply explained by the nature of the surfactant or the viscosity of slurry [35,[37,38]. The order of the viscosity of the slurry was measured by Tu-4 cup viscometer by recording the time through the discharge spout (4 ± 0.02 mm) at room temperature [39]. High viscosity was observed for slurry of SPs, BCs, AKw, these slurries showed high viscosity that is outside the range of the Tu-4 cup method (far more than 150s). Furthermore, slurry of SPs and BCs showed extremely high viscosity which was unable to flow out continuously. And slurry of SPs takes more time than BCs for 10 drops. Therefore, the order of flow time for the slurry (z = 0) is: (SPs > BCs □ K12s≈JFCs> POs> AKs>PMGH). Simultaneously, the viscosity of slurry (z = 11) with additional H_2O was also tested. The order of flow time is (AKw □ BCw > SPw> K12w> JFCw> POw). As can be seen, there is no obvious correlation between the pore characteristics and the viscosity. It should be noted that the viscosity of slurry is dynamic, and more investigation should be performed for the rheological property of the foamed slurry.

Several theories (early mechanical–dynamical stability theory, surface elasticity theory by Gibbs, surface elasticity theory by Marangoni, thin film model theories, etc.) were developed to elaborate the mechanism of foam stability [35,[37,38]. As there are lots of factors (viscosity (bulk and surface), surface occupancy, elasticity for surfactant solution, gravity drainage, capillary suction, and foam films etc.) under static and/or dynamic conditions that affect the final pore characteristics. Furthermore, the pore characteristics also can be affected by the high alkali condition and exothermic reaction with hardening. Here, the pore formation can be explained by introducing gas into the slurry with surfactant. The air–slurry interfaces are generated and rapidly covered by surfactant molecules. And the foam stability plays a major role in the final pore characteristics. Take porous samples obtained by K12 for example, Figure 6 schematically

exhibited three stages (formation, coalescence, and solidification) for air bubbles in the constantly changing foamed slurry. The three stages for the air bubbles in the slurry can be applied to explain the porosity increase with the decrease of solid content. As discussed above, the variety of the surfactant is vital for the porous characteristics (pore formation and stabilization). More investigations will have to be performed to further expound the mechanism for the observed behavior.

The data indicate that the AK surfactant led to high porosity (77vol%; z = 11), while the K12 surfactant led to large cell size (d = 316 μm; z = 11). The decrease of solid content in the slurry (z from 0 to 11) is beneficial to producing more bubbles in the slurry (Figure 6). And different types of surfactants showed various growth trends of total porosity. About 25% increase in the ε was achieved to the K12 surfactant, simultaneously, only ~8% growth was calculated to the PO surfactant with the decrease of solid content in the slurry. The increasing trend of porosity using different types of surfactant with the decrease of solid/liquid ratio is consistent with the pore morphology (Figures 2–4 and Figure 6). The total porosity of PMGs using PO, JFC, SP as surfactant showed obvious lower than samples obtained by AK, K12, BC as surfactant whether the solid content at high level (z = 0) or low level (z = 11). The porosity data is consistent with the pore morphology observed by optical (Figure 2(a); Figure 4(a, a)) and SEM (Figure 2(d, g); Figure 4(d, g) and (d, g)) microscopy. It seems that these three surfactants (PO, JFC, SP) show pretty low foaming ability for the slurry especially when the solid content at high level(z = 0). The result can be further confirmed by the microstructure (Figure 2(a,d,g) and Figure 4 ((a,d,g);(a,d,g))). The bulk density showed inverse results to the total porosity, as expected.

Furthermore, for PMGs obtained using the AK surfactant at high solid content in the slurry (z = 0), several smaller pores were observed in the cell walls and the struts (see Figure 3(d,g)), and these smaller pores can not be observed when the solid/liquid ratio decrease, as can be seen in Figure 3(f,i). These results indicate that the type of surfactant selected for the foaming can have a significant influence on the pore characteristics of the geopolymer components obtained by direct foaming, and that the solid/liquid ratio in the slurry has also had an important effect.

The combination of surfactants with a chemical pore-foaming agent was tested to investigate the synergistic effect on the porous characteristics of PGs. For comparison purposes, a sample (PMGH, Figure 5(a-c), x = 0; y = 11; z = 0) was obtained only using the chemical blowing agent, to highlight the effect of SAs. As evident in Figure 5(a, b), a cellular structure with thick cell wall was obtained, confirming that a porous structure is formed by the decomposition reaction of hydrogen peroxide. The decomposition of hydrogen peroxide enabled the production of geopolymer with a total porosity (ε) of ~62.58 vol%, compressive strength of ~14.76 MPa, and thermal conductivity of ~0.20 W/mK and possessing an average cell size of ~321 μm. These results are in line with previous data obtained using H_2O_2 only as pore-forming agent [5,9].

Figures 2–4((b,e,h) and (B,E,H)) illustrate the morphological features and the cell size distribution of the PGs obtained with different types of SA and fixed H_2O_2 content (y = 11). With the addition of H_2O_2, the porosity increased significantly, and large spheroidal cells surrounded by relatively thick struts were

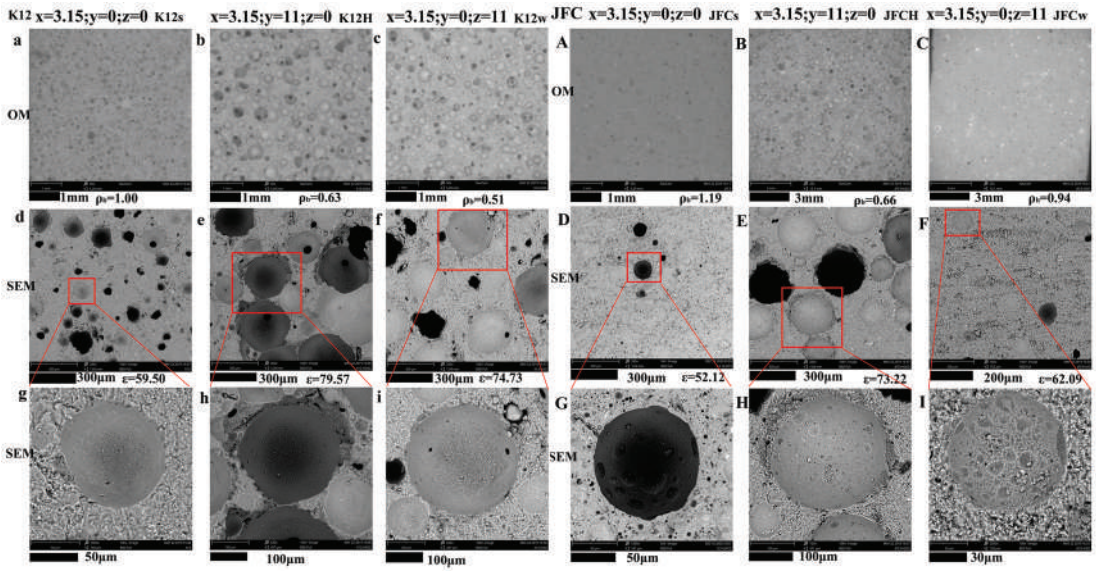

Figure 2. Morphology of the PMGs using K12 (a-i) or JFC (A-I) as stabilizing agents/surfactants and by adding a combination of CPFA (H_2O_2) and stabilizing agents.

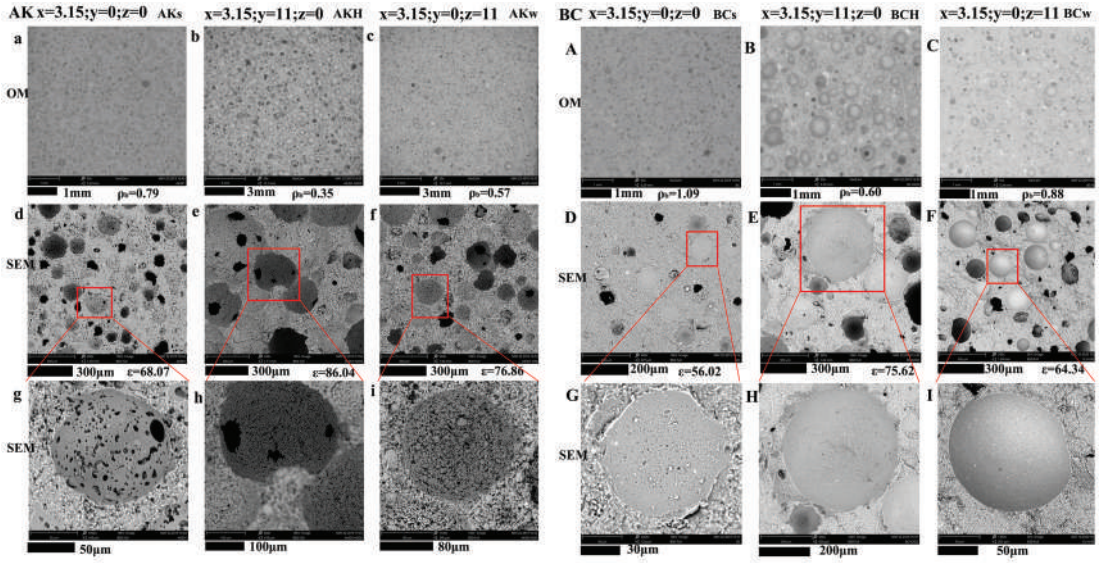

Figure 3. Morphology of the PMGs using AK (a-i) and BC (A-I) as stabilizing agents/surfactants and by adding a combination of CPFA (H_2O_2) and stabilizing agents.

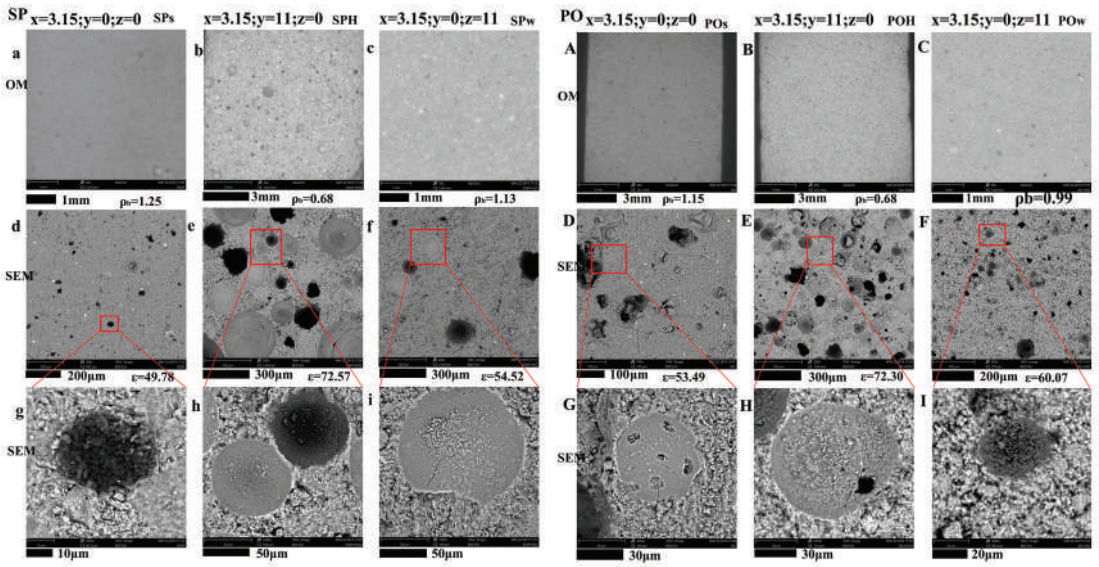

Figure 4. Morphology of the PMGs using SP (a-i) and PO (A-I) as stabilizing agents/surfactants and by adding a combination of CPFA (H_2O_2) and stabilizing agents.

observed. The total porosity (ε/vol%) varied following this order: AKH (86) > K12H (80) > BCH (76) > JFCH (73) ≥ SPH (73) > POH (72). The data showed almost the same order, except for soap(SP) and oil(PO) SAs at the same solid/liquid ratio (y = 0; z = 11), accompanied with increase in porosity of about 20% in comparison to samples obtained using only SAs (y = 0; z = 0). Simultaneously, a ~ 10% porosity increase was detected for PMGs obtained by these four surfactants AK, BC, PO, JFC comparing samples with SAs and additional water added (y = 0; z = 11), and maximum porosity increase (~19%) and minimum porosity increase (~5%) were achieved by SP surfactant and K12 surfactant, respectively.

As it can be seen, the number of bubbles (cells) decreased and their average cell size increased, confirming that O_2 gas evolution by the decomposition of hydrogen peroxide created several large bubbles (cells) in the slurry. Compared with the sample (PMGH, ε = 62.58 vol%), the combination of SAs and hydrogen peroxide in the geopolymer stabilized and enabled the retention of the gas bubbles rather than having them escaping from the slurry (Figure 6). The average cell size (d/μm) of PGs obtained by adding different types of SAs in combination with H_2O_2 showed the same trend with the ε of porous specimens with only SAs added (y = 0; z = 0): AKH (391) > K12H (375) > BCH (362) > JFCH (336) > SPH (243) >POH (111). For the PGs produced by stabilizing agent AK and stabilizing agent K12, smaller pores in the cell wall were also observed in SEM images in Figure 2(e,h) and Figure 3(e,h), which were also detected in previous

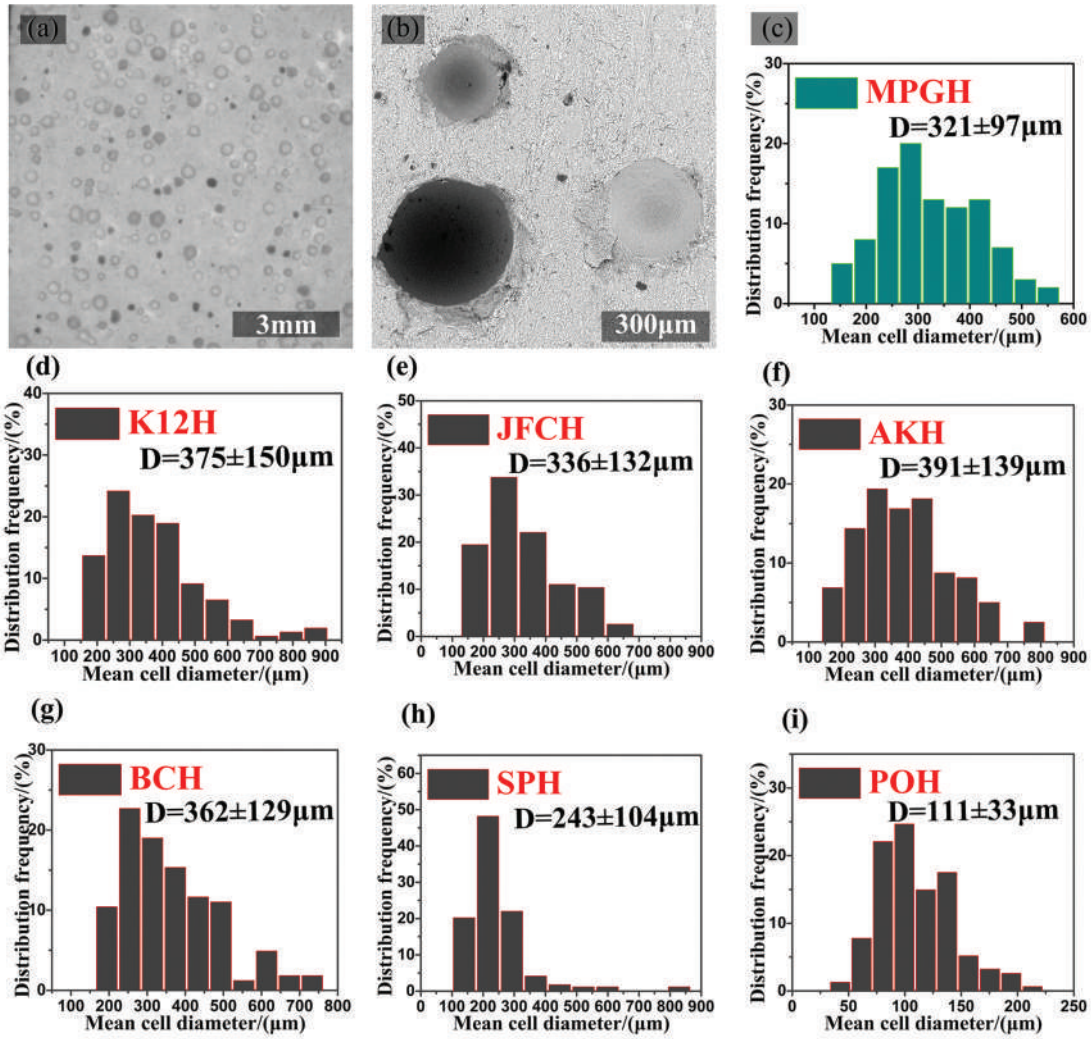

Figure 5. Optical (a) and SEM (b) image and average cell size distribution (c) of the PMGs obtained only by adding CPFA (H_2O_2); average cell size distribution (d-i) of samples produced by adding a combination of CPFA (H_2O_2) and stabilizing agents.

works [5,17]. A relatively homogeneous distribution of micro pores in the geopolymer matrices can be observed from micrographs (Figures 2–4 (b,e,h) and (b,e,h)), and specific evidence is presented in Figure 5 (d-i). From above-mentioned results, it showed that different types of surfactants/stabilizing agents (cationic, anionic, amphoteric, and nonionic etc) were effective to obtain foam slurry at high alkaline solution using designed geopolymer composition with appropriate curing process. A large amount of processing parameters (rheology, chemistry of surfactants, mixing speed, activating solution, curing conditions etc.) using different surfactants/stabilizing agents is still to be explored to further elucidate the reason for the observed behavior.

3.3. Porosity, compression strength, and thermal conductivity

Previous works reported that both mechanical and thermal conductivity properties of porous geopolymers bear a close correspondence to the volume of pores (relative density), pore structure and size, composition, etc [1,11,40]. Figures (7–8) report the compression strength (σ) and thermal conductivity (λ) as a function of the total porosity (ε) for samples investigated in this work and published data for porous metakaolin-based geopolymers (PMGs) produced by adding only chemical blowing agents (H_2O_2, Si, Al), or only stabilizing agents/surfactants, or by adding a combination of blowing agents and stabilizing agents. The PMGs were manufactured using only a chemical blowing agent (H_2O_2) [1,9,11,41], or either Tween 80 (TW) [9], egg white (EW) [5], vegetable protein [42], canola oil (CO), sunflower oil (SO), olive oil (OO) [11], SDS [34], or cetyltrimethyl ammonium bromide [36] as surfactant, with or without chemical-blowing agents. Potassium-based porous geopolymers were produced using only surfactants (EWs) [5], (TWs) [9], (OO, SO, CO) [11], or by adding a combination of hydrogen peroxide and surfactants (EWH) [5], (TWH) [9], (OOH) [11], or only with chemical-blowing agents (H_2O_2) such as (SH-5 [5], SH-9 [9]). PMGs developed in this work possessed mechanical properties very close

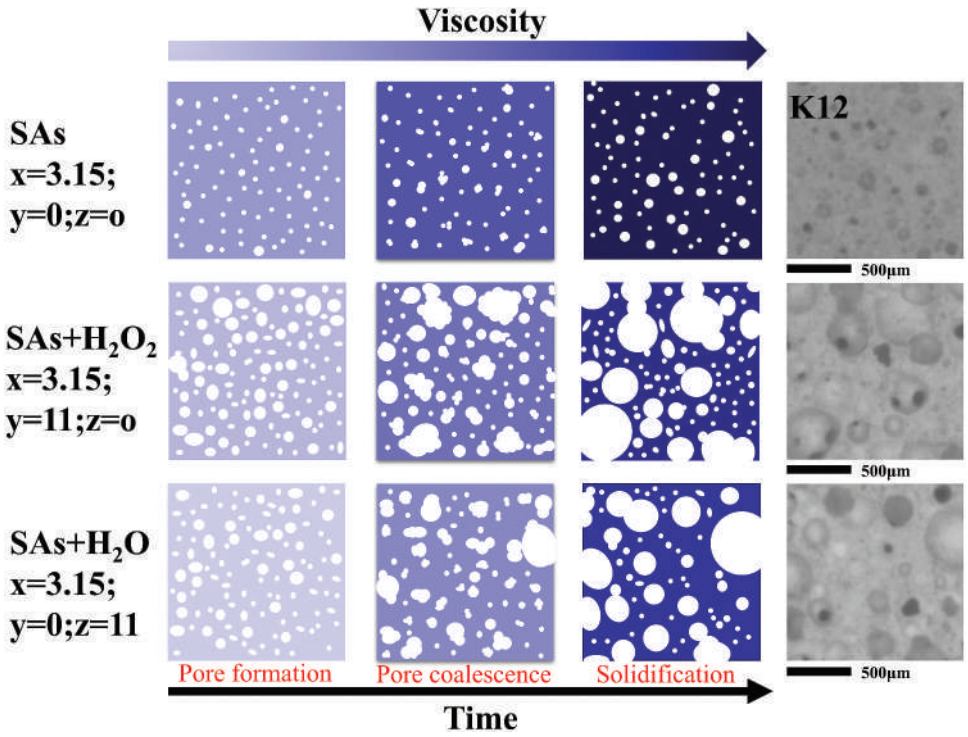

Figure 6. The schematic diagram of the stage of air bubbles (during pore generation and solidification) in the constantly changing geopolymer slurry. Final pore structure was deriving form samples using K12 as surfactant.

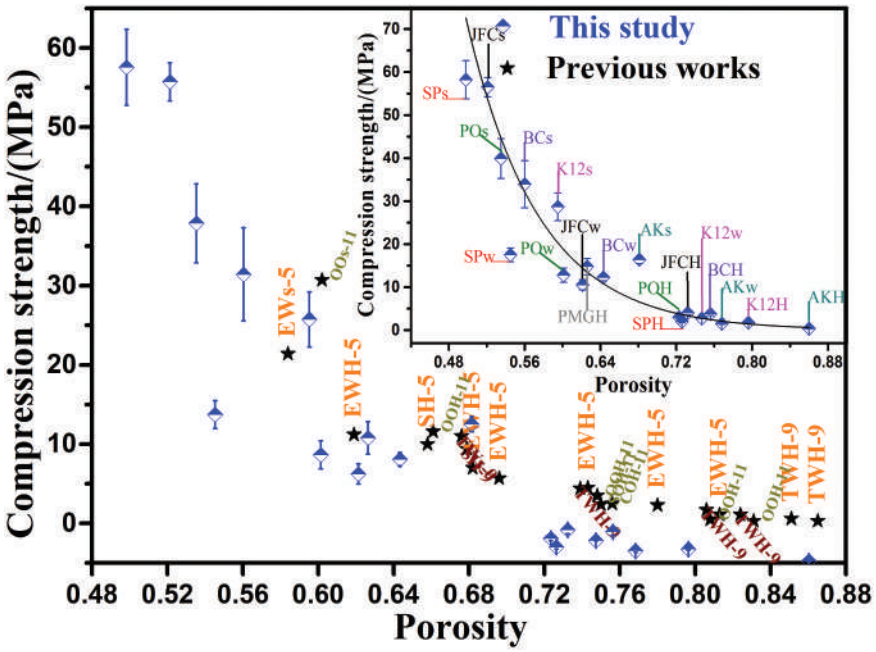

Figure 7. Compression strength vs. total porosity of MK-based PGs made with various SAs or together with CPFA, and samples only with H_2O_2 in this study and previous works (★). Inset figure represents the MK-based porous samples with data points in this work. Data points of previous works(★) are labeled with the corresponding abbreviation of surfactants or chemical pore-forming agents combining with the reference numbers (EW) [5], (TW) [9], (OO) [11].

to the published data for other systems (Figure 7). It is worthy to note that the sodium-based geopolymer usually showed lower mechanical strength than potassium-based geopolymer obtained using a similar procedure [43]. Furthermore, compression stress–strain curve of specimen is showed in **Figs. S(1–6)**. A typical-jagged stress–strain curve beyond the peak was observed when the total porosity higher than 70vol %, which can be used to confirm the high-porosity structure as the successive crushing of pore layers [27,[44,45]. Simultaneously, the variation of elasticity modulus (E) as a function of the total porosity (ε) was presented in **Fig. S7**. Unlike the σ with the ε, there was no obvious relationship between E and ε. However,

when the porosity higher than 70vol%, an exponential decrease trend of E was showed with the increased total porosity(ε) as well. More works will be done to further expound the correlation between mechanical properties to pore characteristics.

With respect to thermal insulation capacity, a comparison between the PMGs produced in this study and data reported for various porous geopolymers manufactured using metakaolin as main raw materials and direct foaming is reported in Figure 8. Porous metakaolin-based geopolymers with ε between 30 and 70 vol% and with λ about 0.15–0.6 W/mK were produced only using Al as chemical pore-foaming agent (CPFA) [40]. High porosity (65–85 vol%) and low λ (0.12–0.33 W/mK) porous geopolymer were produced using silica fume and metakaolin as starting materials, and silica fume also acted as CPFA [46,47]. For PGs with ε between 45 vol% and 90 vol%, the value for λ varied from 0.09 to 0.42 W/mK, consistent with the data reported in other works [5,11,40,46,47].

A simple physical property-porosity model based on minimum solid area (MSA), proposed by Rice [48–50], was used to describe the relationship between total porosity (ε/vol%) and compression strength (σ/MPa). The MSA model, assuming that the mechanical strength of porous materials depends on the MSA fraction of the fracture surface, can be simply expressed by the following equation:

$$\sigma = \sigma_0 exp(-b_1\varepsilon) \tag{3}$$

where σ_0 is the zero-porosity strength, b_1 a characteristic constant which can be correlated with the pore characteristics and ε the total porosity. A high correlation factor R^2 (0.95) was calculated via fitting the obtained ε and σ with Equation (3) (see, inset of Figure 7), demonstrating that the relationship between σ and ε can be well explained by the MSA model when the porosity ranges from □45 vol% to □90 vol%. The compression strength of porous geopolymers decreases exponentially with increasing the total porosity, as demonstrated also by previous investigations [1,5]. A possible explanation for the well-fitting results with the MSA model is that the cell shape can be regarded as quasi-spherical [50].

The physical property-porosity model (MSA) can be applied not only to the stress-determined performance (here, compression strength, σ), but also to the flux-determined performance (here, thermal conductivity, λ) [48]. The corresponding equation can be thus modified to:

$$\lambda = \lambda_0 exp(-b_2\varepsilon) \tag{4}$$

where λ_0 is the zero-porosity thermal conductivity and b_2 is a characteristic constant. A relatively high correlation factor R^2 (0.90) was obtained via fitting the obtained ε and λ with Equation (4) (see, Figure 9(a)), which indicated that the correlation between λ and ε can also be described with sufficient accuracy by the MSA model.

Furthermore, to better predict the variation between ε and λ for materials which can be regarded as comprised of two components, or two phases, five fundamental analytical models (Parallel, Series, Maxwell-Eucken 1 and 2, and Effective Medium Theory) were proposed. However, the normal above-mentioned five models, which assume a certain relatively ideal physical structure, are not well suited to describe the actual pore structure of stochastic porous

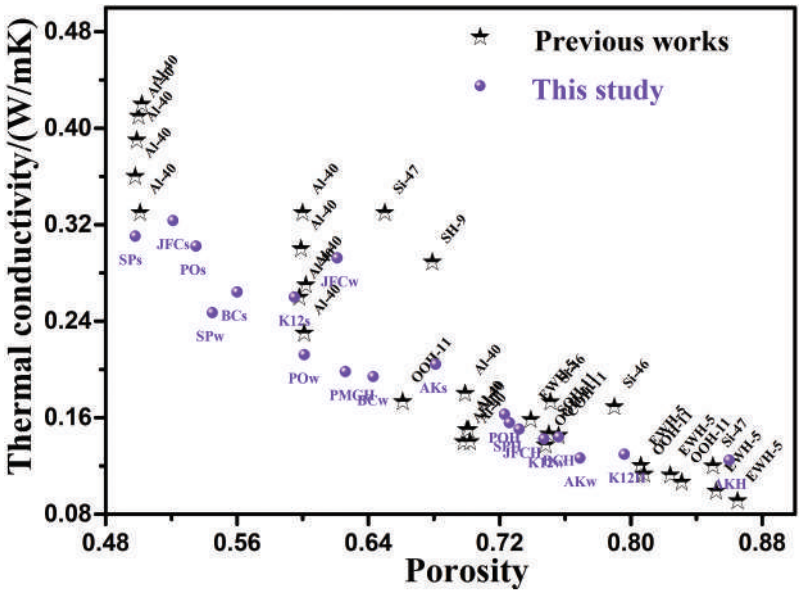

Figure 8. Thermal conductivity vs. total porosity of MK-based PGs made with various SAs or together with CPFA, and samples only with H_2O_2 in this study and previous works. Data points of previous works are labeled with the corresponding abbreviation of surfactants or chemical pore-forming agents combining with the reference numbers(EW) [5], (TW) [9], (OO) [11], (Al) [40],(Si) [46], (Si) [47].

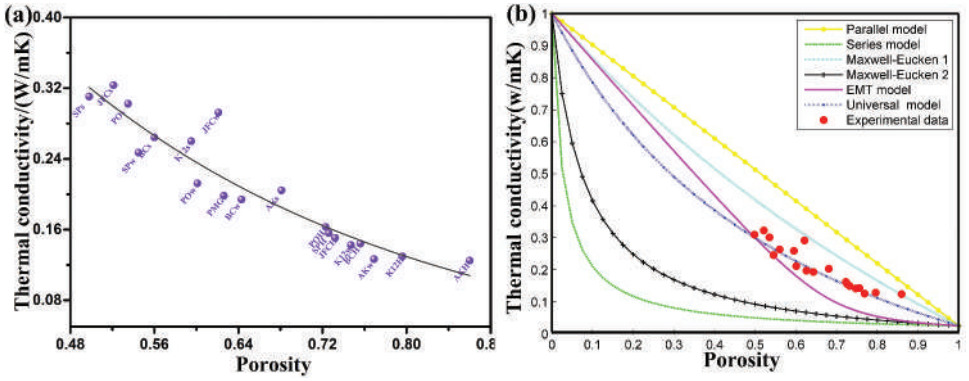

Figure 9. (a)Variation of the experimental λ data as a function of ε, and (b) the correlation obtained following the five fundamental models and the universal model.

materials, such as foams. A new effective medium theory model, which can also be named as an universal model, was proposed based on the five fundamental models [51,52]. The universal model can be expressed using a unifying algebraic equation:

$$\lambda = \frac{\sum_{i=1}^{m} \lambda_i V_i((d_i k')/(d_i - 1)k' + \lambda_i)}{\sum_{i=1}^{m} V_i((d_i k')/(d_i - 1)k' + \lambda_i)}\lambda = \frac{\sum_{i=1}^{m} \lambda_i V_i((d_i k')/(d_i - 1)k' + \lambda_i)}{\sum_{i=1}^{m} V_i((d_i k')/(d_i - 1)k' + \lambda_i)} \quad (5)$$

where λ and V are the thermal conductivity and porosity, subscripts i represent phase i or component I, and m is the total number of components (phases), d_i is a parameter which may be correlated with both component shape and number of Euclidean dimensions, and k′ is a parameter which could be used to reflect the heat conduction between solid (geopolymer) and air [51,52] (according to previous investigations, we can consider k′ = 0.3 [11,53]). In this work, the PGs can be regarded as comprised of two components (m = 2, V_1+ V_2 = 1), i.e., air bubbles (λ_1 = 0.026 W/mK, component 1, V_1) dispersed into a geopolymer matrix (λ_2 = 1.0 W/mK, components 2, V_2) [11]. As it can be seen from the morphology (Figures 2–4), the dispersed phase (air) is spherical or quasi-spherical, and is contained within the uniform medium (geopolymer matrix), thereby d_i is chosen to be 3 [11,53,54].

In Figure 9(b), the thermal conductivity (λ) experimental data as a function of the total pore volume of PMGs obtained by adding only chemical blowing agents (H_2O_2), or only stabilizing agents/surfactants, or by adding a combination of hydrogen peroxide and stabilizing agents are compared with the correlations provided by the five analytical models and the universal model. The experimental data are better described by the universal model, although some deviation and fluctuation were observed. The variation between obtained data and the universal model indicates that the PMGs have complex pore structures. i.e., more than two forms of five basic structures could be found in the porous geopolymer [53]. Furthermore, an additional explanation for the deviation and fluctuation is due to the presence of some cracks (branching, bridging etc.) and [48] photon scattering of the lattice by the nano/meso-pores [54]. Anyhow, the universal model appears to be the most appropriate in predicting the variation of the effective thermal conductivity (λ) with total porosity.

4. Conclusions

Metakaolin-based porous geopolymers were synthesized by direct foaming. The effects of surfactants/stabilizing agents and solid loading on their microstructural characteristics, density, porosity, thermal conductivity, and compression strength were systematically investigated. This study clearly enables following conclusions to be obtained.

(1) Porous geopolymers (PGs) with high porosity (~50 < ε < ~86 vol%), low bulk density (0.35< ρ_b < 1.2 g/cm^3), various average cell size (~101 μm< d <~374 μm), acceptable compression strength (0.35 < σ < 56.5 MPa), and low thermal conductivity (0.13 < λ < 0.32 W/mK) were successfully prepared by direct foaming adding only different types of stabilizing agents/surfactants, or by adding a combination of blowing agents(H_2O_2) and stabilizing agents.

(2) The types of surfactants/stabilizing agents significantly influence the pore microstructure of PGs fabricated by direct foaming.

(3) The minimum solid area (MSA) model can be used to predict the relation between σ or λ and ε.

(4) A unifying equation (universal model), derived from the five fundamental effective thermal conductivity structural models (Series, Parallel, Maxwell–Eucken 1 and 2, EMT), was found to be more accurate for analytically describing the variation between λ and ε of PGs with various pore structure.

The porous geopolymers developed in this work, possessing acceptable strength and low thermal

conductivity, which can be tuned by various surfactants/stabilizing agents, are promising candidates as thermal barriers for the building industry.

Acknowledgments

This work was supported by the Fundamental Research Funds for the Central Universities (3072019CFJ1003; 3072020CF1001), Heilongjiang Postdoctoral Science Foundation Funded Project (LBH-Z19051), and Scientific Research Foundation for the Returned Overseas Chinese Scholars of Heilongjiang Province (2019QD0002).

Disclosure statement

The authors declare that they have no conflict of interest.

Funding

This work was supported by the Fundamental Research Funds for the Central Universities [3072020CF1001;3072019CFJ1003]; Heilongjiang Provincial Postdoctoral Science Foundation [LBH-Z19051]; National Natural Science Foundation of China [52002090]; Scientific Research Foundation for the Returned Overseas Chinese Scholars of Heilongjiang Province [2019QD0002].

ORCID

Chengying Bai http://orcid.org/0000-0003-2555-2330
Paolo Colombo http://orcid.org/0000-0001-8005-6618

References

[1] Bai C, Colombo P. Processing, properties and applications of highly porous geopolymers: a review. Ceram Int. 2018. DOI:10.1016/j.ceramint.2018.05.219
[2] Singh B, Ishwarya G, Gupta M, et al. Geopolymer concrete: A review of some recent developments. Constr Build Mater. 2015. DOI:10.1016/j.conbuildmat.2015.03.036
[3] Lemougna PN, Wang K, Tang Q, et al. Recent developments on inorganic polymers synthesis and applications. Ceram Int. 2016;42:15142–15159.
[4] Ge Y, Yuan Y, Wang K, et al. Preparation of geopolymer-based inorganic membrane for removing Ni2+ from wastewater. J Hazard Mater. 2015;299:711–718.
[5] Bai C, Colombo P. High-porosity geopolymer membrane supports by peroxide route with the addition of egg white as surfactant. Ceram Int. 2017;43:2267–2273.
[6] Belleville P, Pereira F, Ement CL. Hierarchically structured transparent hybrid membranes by in situ growth of mesostructured organosilica in host polymer. Nat Mater. 2006;5:17–19.
[7] Novais RM, Buruberri LH, Seabra MP, et al. Novel porous fly-ash containing geopolymer monoliths for lead adsorption from wastewaters. J Hazard Mater. 2016;318:631–640.
[8] Ge Y, Cui X, Kong Y, et al. Porous geopolymeric spheres for removal of Cu(II) from aqueous solution: synthesis and evaluation. J Hazard Mater. 2015;283:244–251.
[9] Bai C, Franchin G, Elsayed H, et al. High-porosity geopolymer foams with tailored porosity for thermal insulation and wastewater treatment. J Mater Res. 2017. DOI:10.1557/jmr.2017.127
[10] Zhang Z, Provis JL, Reid A, et al. Mechanical, thermal insulation, thermal resistance and acoustic absorption properties of geopolymer foam concrete. Cem Concr Compos. 2015;62:97–105.
[11] Bai C, Ni T, Wang Q, et al. Porosity, mechanical and insulating properties of geopolymer foams using vegetable oil as the stabilizing agent. J Eur Ceram Soc. 2018;38:799–805.
[12] Masi G, Rickard WDA, Vickers L, et al. A comparison between different foaming methods for the synthesis of light weight geopolymers. Ceramics International [Ceram Int.] 2014;40:13891–13902.
[13] Zhang ZH, Zhu HJ, Zhou CH, et al. Geopolymer from kaolin in China: an overview. Appl Clay Sci. 2016;119:31–41.
[14] Bai C, Li H, Bernardo E, et al. Waste-to-resource preparation of glass-containing foams from geopolymers. Ceram Int. 2019. DOI:10.1016/j.ceramint.2018.12.227
[15] Korat L, Ducman V. The in fl uence of the stabilizing agent SDS on porosity development in alkali-activated fl y-ash based foams. Cem Concr Compos. 2017;80:168–174.
[16] Liu Y, Yan C, Zhang Z, et al. A facile method for preparation of floatable and permeable fly ash-based geopolymer block. Mater Lett. 2016;185:370–373.
[17] Masi G, Rickard WDA, Vickers L, et al. A comparison between different foaming methods for the synthesis of light weight geopolymers. Ceram Int. 2014;40:13891–13902.
[18] Liu Z, Shao NN, Wang DM, et al. Fabrication and properties of foam geopolymer using circulating fluidized bed combustion fly ash. Int J Miner Metall Mater. 2014;21:89–94.
[19] Liu Z, Shao N, Huang T, et al. Effect of SiO 2/Na 2 O mole ratio on the properties of foam geopolymers fabricated from circulating fluidized bed fly ash. Int J Miner Metall Mater. 2014;21:620–626. .
[20] Ze LIU, Ning-ning S, Jun-feng QIN, et al. Strength and thermal behavior of low weight foam geopolymer using circulating fluidized bed combustion fly ash. J CENT SOUTH UNIV. 2015;1–8. DOI:10.1007/s11771-015-2904-0.
[21] Samson G, Cyr M, Gao XX. Thermomechanical performance of blended metakaolin-GGBS alkali-activated foam concrete. Constr Build Mater. 2017;157:982–993.
[22] Samson G, Cyr M, Samson G, et al. Porous structure optimisation of flash-calcined metakaolin/fly ash geopolymer foam concrete geopolymer foam concrete. Eur J Environ Civ Eng. 2017;8189:0.
[23] Zhang W, Ma Q, Zeng K, et al. Mechanical properties and thermal stability of carbon fiber cloth reinforced sol-derived mullite composites. J CENT SOUTH UNIV. 2019;8:218–227.
[24] Liu J, Huo W, Zhang X, et al. Optimal design on the high-temperature mechanical properties of porous alumina ceramics based on fractal dimension analysis. J Adv Ceram. 2018;7:89–98.
[25] Cosn M. Monodisperse CoSn 2 and FeSn 2 nanocrystals as high-performance anode materials for lithium-ion batteries †. Nanoscale. 2018;6827–6831. DOI:10.1039/c7nr08261d.
[26] Alsn T, Cai L, Huang Z, et al. Fabrication, mechanical properties, and tribological behaviors of Ti 2 AlC and

Ti2AlSn0.2C solid solutions. J Adv Ceram. 2017;6,90–99. https://doi.org/10.1007/s40145-017-0221-9
[27] Hajimohammadi A, Ngo T, Mendis P, et al. Pore characteristics in one-part mix geopolymers foamed by H2O2: the impact of mix design. Mater Des. 2017. DOI:10.1016/j.matdes.2017.05.084
[28] Hernando L. Influence of blowing agent on the fresh- and hardened-state properties of lightweight geopolymers PhD thesis View project. JMADE. 2016;108:551–559.
[29] Granizo ML, Blanco-Varela MT, Palomo A. Influence of the starting kaolin on alkali-activated materials based on metakaolin. Study of the reaction parameters by isothermal conduction calorimetry. J Mater Sci. 2000;35:6309–6315.
[30] Shiu H, Lin K, Chao S, et al. Effects of foam agent on characteristics of thin-film transistor liquid crystal display waste glass-metakaolin-based cellular geopolymer. ENVIRON PROG SUSTAIN. 2014;33.
[31] Rovnaník P. Effect of curing temperature on the development of hard structure of metakaolin-based geopolymer. Constr Build Mater. 2010;24:1176–1183.
[32] Tchakouté HK, Rüscher CH, Hinsch M, et al. Utilization of sodium waterglass from sugar cane bagasse ash as a new alternative hardener for producing metakaolin-based geopolymer cement. Chemie Der Erde. 2017;77:257–266. .
[33] Bai T, Song ZG, Wu YG, et al. Influence of steel slag on the mechanical properties and curing time of metakaolin geopolymer. Ceram Int. 2018;44:15706–15713.
[34] Kaddami A, Pitois O. Cement and Concrete Research A physical approach towards controlling the microstructure of metakaolin- based geopolymer foams. Cem Concr Res. 2019;124:105807.
[35] Strozi Cilla M, Colombo P, Raymundo Morelli M. Geopolymer foams by gelcasting. Ceram Int. 2014;40:5723–5730.
[36] Petlitckaia S, Poulesquen A. Design of lightweight metakaolin based geopolymer foamed with hydrogen peroxide. Ceram Int. 2019;45:1322–1330.
[37] Pugh RJ. Foaming, foam films, antifoaming and defoaming. Adv Colloid Interface Sci. 1996;64:67–142.
[38] Bureiko A, Trybala A, Kovalchuk N, et al. Current applications of foams formed from mixed surfactant-polymer solutions. Adv Colloid Interface Sci. 2015;222:670–677.
[39] Zhou Y, Hu H, Xu X, et al. High-risk region of bird streamer flashover in high-voltage transmission lines. J Electrostat. 2009;67:311–315. .
[40] Kamseu E, Nait-ali B, Bignozzi MC, et al. Bulk composition and microstructure dependence of effective thermal conductivity of porous inorganic polymer cements. J Eur Ceram Soc. 2012;32:1593–1603.
[41] Palmero P, Formia A, Antonaci P, et al. Geopolymer technology for application-oriented dense and lightened materials. Elaboration and characterization. Ceram Int. 2015;41:12967–12979.
[42] Verdolotti L, Liguori B, Capasso I, et al. Synergistic effect of vegetable protein and silicon addition on geopolymeric foams properties. J Mater Sci. 2014;50:2459–2466.
[43] Xu H, Van Deventer JSJ. The geopolymerisation of alumino-silicate minerals. INT J MINER PROCESS. 2000. DOI:10.1016/S0301-7516(99)00074-5
[44] Shakouri S, Bayer Ö, Erdoğan ST. Development of silica fume-based geopolymer foams. Constr Build Mater. 2020;260. DOI:10.1016/j.conbuildmat.2020.120442.
[45] Luo X, Xu JY, Li W. Basalt fiber reinforced porous aggregates-geopolymer based cellular material. Funct Mater Lett. 2015;8:2–5.
[46] Papa E, Medri V, Kpogbemabou D, et al. Porosity and insulating properties of silica-fume based foams. Energy Build. 2016;131:223–232.
[47] Henon J, Alzina A, Absi J, et al. Potassium geopolymer foams made with silica fume pore forming agent for thermal insulation. J Porous Mater. 2013;20:37–46.
[48] Rice RW. Comparison of physical property-porosity behaviour with minimum solid area models. J MATER SCI. 1996;31.
[49] Rice RW. Comparison of stress concentration versus minimum solid area based mechanical property-porosity relations. J MATER SCI. 1993;28:2187–2190.
[50] Rice RW, Grace WR. Evaluation and extension of physical property-porosity models based on minimum solid area. J MATER SCI. 1996;31.
[51] Wang J, Carson JK, North MF, et al. A new approach to modelling the effective thermal conductivity of heterogeneous materials. INT J HEAT MASS TRAN. 2006;49:3075–3083.
[52] Gong L, Wang Y, Cheng X, et al. International Journal of Heat and Mass Transfer A novel effective medium theory for modelling the thermal conductivity of porous materials. Int J Heat Mass Transfer. 2014;68:295–298.
[53] Zenabou NNM, Benoit-ali N, Zekeng S, et al. Improving insulation in metakaolin based geopolymer Effects of metabauxite and metatalc. J BUILD ENG. 2019;23:403–415.
[54] Guo H, Li W, Ye F. Preparation of microporous mullite ceramics by foaming for high temperature thermal isolation. Ceram Int. 2016;42:17332–17338.